Superconducting Gap Anisotropy vs Doping Level in High-T_c Cuprates

C. Kendziora
Code 6650, Naval Research Laboratory, Washington, D.C. 20375

R. J. Kelley and M. Onellion
Physics Department, University of Wisconsin, Madison, Wisconsin 53706
(Received 6 December 1995)

We report the results of electronic Raman scattering in $Bi_2Sr_2CaCu_2O_{8+\delta}$ (Bi2212) and $Tl_2Ba_2CuO_{6+\delta}$ (Tl2201) high-T_c superconductors with variations in the oxygen content. Near optimal doping, both materials show gap anisotropy, with $2\Delta/k_BT_c$ values of 7.2 (B_{1g}) vs 5.8 (A_{1g}) in Tl2201 and 8.5 (B_{1g}) vs 6.2 (A_{1g}) in Bi2212. However, overdoped samples exhibit a symmetry independent gap with $2\Delta/k_BT_c$ ranging from 5.2 for Bi2212 ($T_c = 57$ K) to 3.9 in Tl2201 ($T_c = 37$ K). We compare the data with calculations using both isotropic *s*-wave and *d*-wave order parameters. [S0031-9007(96)00724-7]

PACS numbers: 74.25.Gz, 74.62.Dh, 74.72.Hs, 78.30.Er

Anisotropy of the superconducting gap within the CuO_2 planes of the cuprates has been observed using several experimental techniques [1–5]. This behavior is in general agreement with the predictions of models based on *d*-wave or anisotropic *s*-wave pairing. Our previous results of electronic Raman scattering (ERS) [6] and angle resolved photoemission [4] have shown that such gap anisotropy is a function of doping in $Bi_2Sr_2CaCu_2O_{8+\delta}$ (Bi2212); similar effects have been seen in $YBa_2Cu_3O_{7-\delta}$ [7,8]. In this Letter, we expand the range of doping available through oxygen intercalation and show that the gap becomes symmetry independent in highly overdoped crystals. Furthermore, we demonstrate that the coupling strength decreases dramatically, from a very strong-coupling value of $(6-8)k_BT_c$ in optimally doped materials to a nearly weak-coupled value of $3.9k_BT_c$ in overdoped $Tl_2Ba_2CuO_{6+\delta}$ (Tl2201).

Bi2212 crystals used in this study were grown using a self-flux technique [9,10]. These crystals were postannealed in a high oxygen pressure to intercalate excess oxygen and raise the hole-type carrier concentration [10,11] while reducing T_c from 90 to 57 K. The Tl2201 crystals were prepared by partially melting a stoichiometric mixture of Tl_2O_3, BaO_2, and CuO in crimped gold tubing at 900 °C in flowing oxygen. As grown, $T_c = 78$ K ($\Delta T_c = 5$ K), indicating these crystals are slightly overdoped relative to the optimal T_c of 90 K in this material. When postannealed in an oxygen atmosphere, T_c of these crystals (reversibly) decreases to 37 K ($\Delta T_c = 2$ K). Such samples of both Bi2212 [10,11] and Tl2201 [12] show 50% lower resistivity (ρ) at room temperature and $\rho(T) \propto T^2$ characteristic of overdoped cuprates.

Raman scattering measurements were made using the 514.5 nm line of an Ar^+ laser at incident power densities of 3–20 W/cm. The laser heating was estimated to be 5–20 K above ambient by comparing the ratio of Stokes and anti-Stokes spectra [13]. The scattered light was dispersed with a resolution of 9 cm^{-1} and detected by a cooled charge coupled device array.

At room temperature, all of the cuprates show a background in Raman spectroscopy due to scattering from the electronic continuum. Superimposed on top of this are sharp phonon excitations. Through an appropriate choice of incident and scattered polarization vectors, it is possible to isolate the behavior of both phonons and electrons of certain symmetries within a given crystal.

For the purposes of selection rule analysis, the polarizations of incident and scattered light are usually indexed with X and Y taken parallel to the Cu-O bonds. In the D_{4h} point group, *a*-*b* plane Raman scattering (with light propagating parallel to the crystal *c* axis) measured in the $Z(XY)\overline{Z}$ polarization samples the B_{2g} component, while $Z(XX)\overline{Z}$ samples a combination of the A_{1g} and B_{1g} symmetries. If X' and Y' denote axes rotated by 45° from X and Y, then $Z(X'Y')\overline{Z}$ couples to excitations of B_{1g} symmetry. For Bi2212, X and Y are indexed along the Bi-O bonds, rotated by 45° with respect to the Cu-O bonds. In this case, XY polarization samples B_{1g} symmetry, $X'Y'$ samples B_{2g}, and XX couples to $(A_{1g} + B_{1g})$.

Recent theoretical work has shown that ERS from different symmetries can reveal gap anisotropy [1415]. Although experiments measure an average over the entire Fermi surface (FS), certain angles are weighted more heavily in the integration. To illustrate this we note that in high-T_c cuprates intraband electronic Raman scattering is dominated by fluctuations in the effective mass around the FS given by the equation $\epsilon(\mathbf{k}) = 0$. In the limit where the wave-vector transfer $\mathbf{q} \rightarrow 0$ we follow the calculations of Klein and Dierker [16] to arrive at an expression for the Raman scattering efficiency:

$$\frac{d^2S}{d\omega\, d\Omega} = \frac{r_0^2 \hbar N(E_F) m^2}{\omega}\left[\frac{\langle \gamma^{-2}\lambda\rangle - \langle \gamma^{-1}\lambda\rangle^2}{\langle \lambda\rangle}\right]''. \quad (1)$$

In this equation, ω is the frequency of Raman shift, Ω the solid angle scattered through, r_0 the Thomson radius of the electron, $N(E_F)$ the density of states at the Fermi level, and m the mass of the bare electron. The symbols

$\langle\,\rangle$ indicate that the quantity within is integrated around the entire FS. λ is a complex function, the imaginary part of which is given by

$$\lambda = \frac{4|\Delta(\mathbf{k})|^2}{\sqrt{\omega^2 - 4|\Delta(\mathbf{k})|^2}}, \qquad (2)$$

with the restriction that $\omega^2 > 4\Delta^2(\mathbf{k})$. Equation (2) clearly shows that ERS is insensitive to the sign of the gap. In Eq. (1), γ is the Raman vertex, given for each polarization by

$$\gamma_{ij}(\mathbf{k}) = \frac{m}{\hbar^2}\, e^I \frac{1}{m^*} e^S = \frac{m}{\hbar^2} \sum_{i,j} e_i^I \frac{\partial^2 \epsilon(\mathbf{k})}{\partial k_i \partial k_j} e_j^S, \qquad (3)$$

where $I \equiv$ incident and $S \equiv$ scattered.

Figure 1(a) depicts a tight binding FS [15,17,18] where

$$\epsilon(\mathbf{k}) = 2t[\cos(k_x a) + \cos(k_y a)] - 4s[\cos(k_x a)\cos(k_y a)] + \mu, \qquad (4)$$

with $t = -1$, $s = 0.3$, and $\mu = 1.16$. The angular dependence (including the sign) of the A_{1g} symmetry is displayed in the polar plot of Fig. 1(b). Figures 1(c) and 1(d) show the angular weighting functions for B_{1g} and B_{2g}, respectively.

For a given value of ω, the Raman scattering intensity is calculated by integrating the expression in Eq. (1) around the FS with γ for each symmetry and the assumed gap $\Delta(\mathbf{k})$. The second term in Eq. (1) represents the Coulomb screening, which is identically zero for all B_{1g} and B_{2g}. In A_{1g}, however, $\langle\gamma^{-1}\lambda\rangle^2 \neq 0$ and screening prevents the spectra from appearing as a sum of B_{1g} and B_{2g}-like components, as Fig. 1(b) might suggest.

Figure 2 shows Raman scattering data taken in $X'X'$ ($A_{1g} + B_{1g}$) and $X'Y'$ (B_{1g}) polarizations (symmetry) on two samples of Tl2201. The XY (B_{2g}) cross section was negligibly small at this excitation wavelength. Figure 2(a) shows the data for a sample with $T_c = 78$ K, while the sample in Fig. 2(b) had $T_c = 37$ K. The $X'X'$ data have been scaled by 1/4 and offset by the amounts shown so that both polarizations can be compared. The normal state (N) spectra are drawn with dashed lines; solid lines represent the superconducting state (S). Each curve has been adjusted for the Bose factor at the temperatures of Fig. 2(a): 90 K (N) and 30 K (S); Fig. 2(b): 50 K (N) and 20 K (S). Rayleigh scattering due to sample roughness causes the spectra to turn up at low frequency in $X'X'$.

The effect of superconductivity on ERS is evident in both samples and in both polarizations. The peaks formed in the continuum (illustrated by arrows) are broadened, due to the excited carriers' finite lifetime. As in previous measurements [19], a polarization dependence is seen in the $T_c = 78$ K sample of Fig. 2(a), with the peak in $X'X'$ centered at roughly 315 cm^{-1} ($5.8k_BT_c$), while the peak in $X'Y'$ is at 390 cm^{-1} ($7.2k_BT_c$).

The effects of excess oxygen (which reduces T_c to 37 K) on the Raman spectra of Tl2201 are shown in Fig. 2(b). Although not the focus of this study, there is a redistribution of phonon strengths and positions in both polarizations. The continuum peaks have also shifted to a much lower energy, 100 ± 5 cm^{-1} ($3.9k_BT_c$) in each polarization, consistent with earlier reports [20]. Rayleigh scattering is the most likely reason the superconducting $X'X'$ spectrum does not cross that of the normal state in Fig. 2(b).

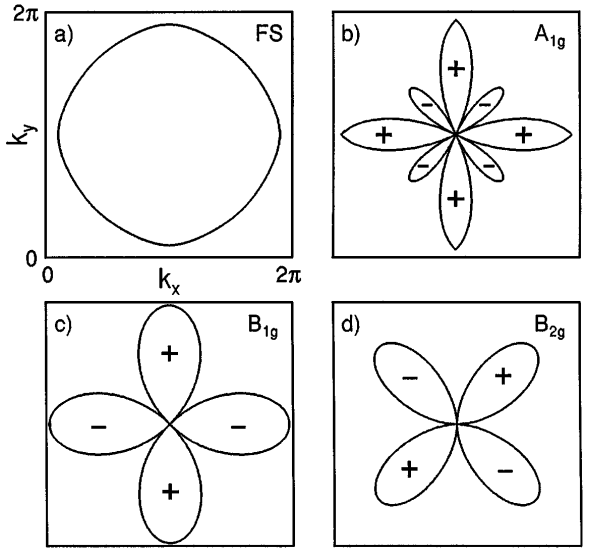

FIG. 1. A polar plot of the angular dependencies of (a) the Fermi surface from Eq. (4), (b) the A_{1g} Raman vertex from Eq. (3), (c) the B_{1g} vertex, and (d) the B_{2g} vertex.

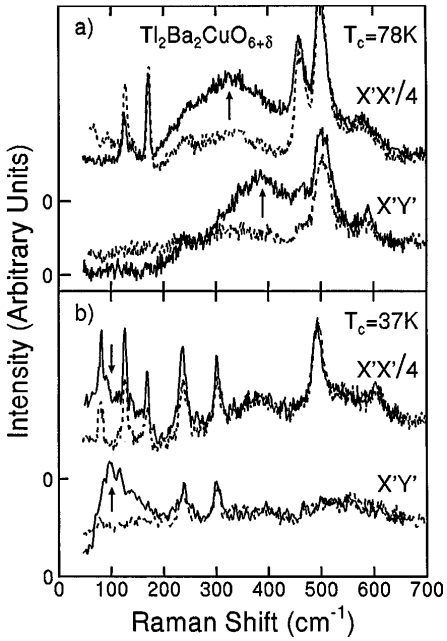

FIG. 2. Raman spectra taken in $X'X'$ ($A_{1g} + B_{1g}$) and $X'Y'$ (B_{1g}) polarizations (symmetry) on Tl2201 with (a) $T_c = 78$ K and (b) $T_c = 37$ K. The $X'X'$ data have been scaled by a factor of 1/4 and offset by the amount shown. The normal state spectra [$T = 90$ K in (a), $T = 50$ K in (b)] are drawn with dashed lines; solid lines show the superconducting behavior [$T = 30$ K in (a), $T = 20$ K in (b)].

Similar behavior is seen as a function of doping in Bi2212. Figure 3 plots Raman scattering spectra for crystals with (a) $T_c = 90$ K and (b) $T_c = 57$ K. The various polarizations have been scaled as indicated in this figure and offset vertically by the amounts shown. All curves have been multiplied by the Bose factor for the temperatures of Fig. 3(a): 100 K (N) and 30 K (S); Fig. 3(b): 70 K (N) and 30 K (S). To emphasize the continuum behavior, the $X'Y'$ and XY curves in Fig. 3(a) as well as the $X'Y'$ in 3(b) have been smoothed.

The $T_c = 90$ K sample exhibits a characteristic gap anisotropy. In XX, which is dominated by scattering of A_{1g} symmetry, the continuum peak is centered at 390 cm^{-1} ($6.2k_BT_c$). The B_{2g} peak is centered at 470 cm^{-1} ($7.5k_BT_c$) while the B_{1g} peak is at 530 cm^{-1} ($8.5k_BT_c$), in general agreement with earlier studies [21–24].

The ERS of Bi2212 changes considerably with excess oxygen. In Fig. 3(b), the continuum peaks have shifted to much lower energies with a sharp onset at low frequencies and a broad tail above the pair-breaking maximum. This suggests that the sample may be "dirty" (characterized by scattering rate $\Gamma \sim \Delta$), in which case a tail up to $8k_BT_c$ would be predicted due to the carriers' finite lifetime [25]. Remarkably, these peaks are at 210 ± 10 cm^{-1} ($5.2k_BT_c$) in all three symmetries. Both the size and polarization independence of the observed superconducting gap were repeatable on other samples.

In Fig. 4, we plot I_S/I_N for Bi2212 from Fig. 3. The ratios have been normalized and offset so that XX and XY can be viewed simultaneously and compared with calculations. Taking this ratio nearly completely removes evidence of the phonons, which were not subtracted. In Fig. 4(a), XX (A_{1g}) and XY (B_{1g}) data for the $T_c = 90$ K sample are compared to calculations of Eq. (1) using a gap [$\Delta(\mathbf{k}) = \cos(2\phi)$] with d-wave symmetry and $2\Delta/k_BT_c = 8.6$. In Fig. 4(b), XX and XY spectra for the $T_c = 57$ K sample are overlaid with a calculation using a broadened isotropic gap $\Delta(k) = 1$ with $2\Delta/k_BT_c = 5.2$.

Three factors affecting the calculated spectra should be noted. (1) To avoid singularities in the calculations, we have employed a Gaussian distribution of gaps (centered at 1) with a full width at half maximum (FWHM) of 0.3 for $T_c = 90$ K, and 0.4 for $T_c = 57$ K. Phenomenologically, this accounts for the finite lifetime of the excited carriers, as well as a range of T_c's much larger than that observed in resistivity or ac susceptibility. This model can thus account for nonzero intensity below 2Δ in the case of an isotropic gap, whereas lifetime effects alone cannot [25]. The introduction of a similar convolution has been necessary to fit tunneling data in the cuprates [5,26,27]. (2) To offset the effects of screening, the calculated A_{1g} was scaled up to the same peak strength as that in B_{1g}, even though the observed XX intensity is stronger than XY. (3) This theory does not account for ERS in the normal state, and thus the calculations decline toward zero for $\omega > 2\Delta$. The insertion of a normal state self-energy component physically related to electron-electron or spin-

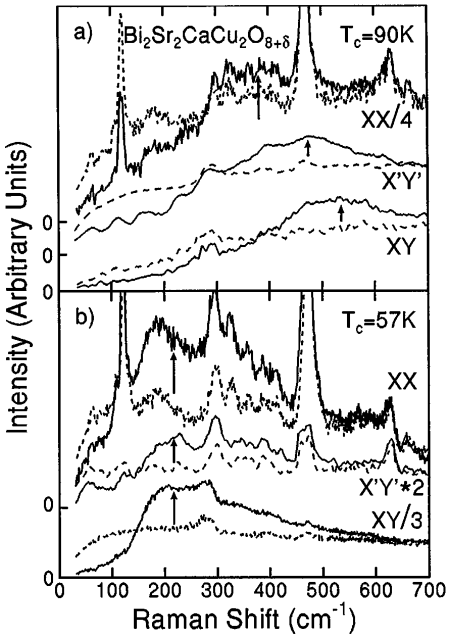

FIG. 3. Raman spectra for Bi2212 with (a) $T_c = 90$ K and (b) $T_c = 57$ K. The spectra have been scaled as indicated in the figure and offset by the amounts shown. The normal state data [$T = 100$ K in (a), $T = 70$ K in (b)] are drawn with dashed lines; solid lines show the superconducting state ($T = 30$ K). The $X'Y'$ and XY curves in (a) and the $X'Y'$ in (b) have been smoothed.

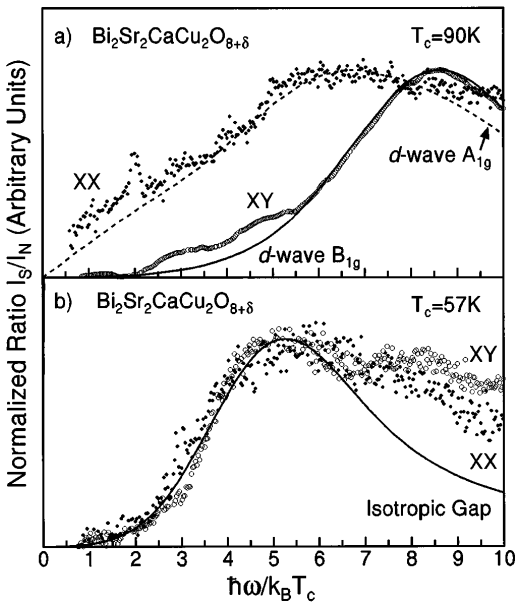

FIG. 4. The ratios I_S/I_N for Bi2212 from Fig. 3. (a) The XX (A_{1g}) and (smoothed) XY (B_{1g}) data for the $T_c = 90$ K sample are compared to the calculations of Eq. (1) using a gap with d-wave symmetry. (b) The XX and XY spectra for the $T_c = 57$ K sample are overlaid with a calculation using a broadened isotropic gap.

fluctuation scattering [28] greatly improves the quality of the fits for $\omega > 2\Delta$.

Spectra from the $T_c = 90$ K sample and the *d*-wave calculations show some remarkable similarities. The model successfully predicts an ω^3 shape in B_{1g} symmetry, as well as the linear extrapolation to zero in A_{1g}. Consideration of a less anisotropic gap without nodes shifts the predicted A_{1g} peak closer to $2\Delta_{\max}$ and suggests that (except for broadening) the low frequency scattering in each symmetry should go to zero at the gap minimum. Irrespective of the FS shape and the exact function assumed for $\Delta(\mathbf{k})$, the ERS spectra of optimally doped crystals demonstrate that the gap (1) is anisotropic, (2) has maxima along $\mathbf{k}_x = 0$ and $\mathbf{k}_y = 0$, and (3) has minima $\ll 2\Delta$.

Devereaux has recently proposed that impurity scattering can distinguish whether the anisotropic gap has nodes required by symmetry [28]. Oxygen is not the ideal impurity for cuprates because of its effect on carrier concentration. Nonetheless, Devereaux's prediction that the peak frequencies should retain their symmetry dependent anisotropy for a *d*-wave but coalesce in the *s*-wave case bears on the observations of Fig. 4(b). Here the ratios of *XX* and *XY* spectra are both fit using the same isotropic gap with broadening. The Tl2201 data in Fig. 2 also display a symmetry independent gap with $2\Delta/k_BT_c = 3.9$, but the Rayleigh scattering from these crystals obscures our measurement of the low frequency behavior for $\omega < \Delta$.

It is crucial to note that the gap does not scale with T_c for any symmetry, but rather decreases with increased doping level to $2\Delta/k_BT_c = 3.9$ (5.2) in samples of Tl2201 (Bi2212) with $T_c = 37$ K (57 K). The symmetry independent gap seen in ERS can be considered characteristic of heavily overdoped cuprates. A nearly isotropic ERS gap ($2\Delta/k_BT_c \approx 4.1$–$4.9$) has been reported in $Nd_{1.85}Ce_{0.15}CuO_4$ [29]. Because at this cerium concentration the resistivity ($\rho \propto T^2$) of this material is typical of the overdoped cuprates [30], we speculate that each cuprate system will manifest a symmetry independent gap at high doping levels. The greatly reduced value of this gap relative to T_c is further evidence that at sufficiently high doping levels the cuprates manifest weak-coupling superconductivity.

In conclusion, we have performed electronic Raman scattering measurements on Bi2212 and Tl2201 with variations in the oxygen content. We compare the observed spectra in the superconducting state with that calculated using order parameters of isotropic *s*-wave and *d*-wave symmetries. Near optimal doping, both materials show a very strong-coupling gap ($2\Delta/k_BT_c \sim 8$) with anisotropic features suggesting nodes. When the carrier concentration is raised, both materials exhibit a symmetry independent gap and $2\Delta/k_BT_c$ values consistent with an *s*-wave order parameter at strengths approaching the weak-coupling limit.

The Tl2201 crystals were provided by T. A. Vanderah of the Ceramics Division, National Institute of Standards and Technology. C.K. acknowledges the support of the National Research Council. R. J. K and M. O. acknowledge support from the NSF.

Note added.—Since the submission of this manuscript, we have become aware of a recent paper by Hackl *et al.* where ERS was measured on an overdoped Bi2212 crystal with $T_c = 55$ K [31]. These authors observed similar symmetry independent gap peaks with a reduced value of $2\Delta/k_BT_c$. However, their observation of a symmetry dependence to the low frequency power laws led them to suggest a persistence of the *d*-wave order parameter into the overdoped phase.

[1] M. Boekholt, M. Hoffmann, and G. Guntherodt, Physica (Amsterdam) **175C**, 127 (1991).
[2] R. J. Kelley *et al.*, Phys. Rev. Lett. **71**, 4051 (1993).
[3] Z.-X. Shen *et al.*, Phys. Rev. Lett. **70**, 1553 (1993).
[4] R. J. Kelley *et al.*, Science **271**, 1255 (1996).
[5] Jeffrey Kane *et al.*, Phys. Rev. Lett. **72**, 128 (1994).
[6] C. Kendziora and A. Rosenberg, Phys. Rev. B **52**, R9867 (1995).
[7] X. K. Chen *et al.*, Phys. Rev. B **48**, 10 530 (1993).
[8] M. Kall *et al.*, Physica (Amsterdam) **235C–240C**, 1095 (1994).
[9] C. Kendziora *et al.*, Phys. Rev. B **45**, 13 025 (1992).
[10] C. Kendziora *et al.*, Physica (Amsterdam) **257C**, 74 (1996).
[11] C. Kendziora *et al.*, Phys. Rev. B **48**, 3531 (1993).
[12] Y. Kubo *et al.*, Phys. Rev. B **43**, 7875 (1991).
[13] A. Maksimov *et al.*, Solid State Commun. **81**, 407 (1992).
[14] T. P. Devereaux *et al.*, Phys. Rev. Lett. **72**, 396 (1994).
[15] D. Branch and J. P. Carbotte, Phys. Rev. B **52**, 603 (1995).
[16] M. V. Klein and S. B. Dierker, Phys. Rev. B **29**, 4976 (1984).
[17] T. P. Devereaux, J. Supercond. **8**, 421 (1995).
[18] X. K. Chen *et al.*, Phys. Rev. Lett. **73**, 3290 (1994).
[19] R. Nemetschek *et al.*, Phys. Rev. B **47**, 3450 (1993).
[20] G. Blumberg *et al.*, Physica (Amsterdam) **235C–240C**, 1137 (1994).
[21] T. Staufer *et al.*, Phys. Rev. Lett. **68**, 1069 (1992).
[22] A. Yamanaka *et al.*, J. Phys. Chem. Solids **53**, 1627 (1992).
[23] D. H. Leach *et al.*, Solid State Commun. **88**, 457 (1993).
[24] A. Hoffmann *et al.*, J. Low Temp. Phys. **99**, 201 (1995).
[25] S. L. Cooper and M. V. Klein, Comments Condens. Matter **15**, 99 (1990).
[26] Qun Chen *et al.*, Phys. Rev. B **49**, 6193 (1994).
[27] T. Becherer *et al.*, Z. Phys. B **86**, 23 (1992).
[28] T. P. Devereaux, Phys. Rev. Lett. **74**, 4313 (1995).
[29] B. Stadlober *et al.*, Phys. Rev. Lett. **74**, 4911 (1995).
[30] Wu Jiang *et al.*, Phys. Rev. Lett. **73**, 1291 (1994).
[31] R. Hackl *et al.* (unpublished).